On-line Magnetic Resonance Quality Evaluation Sensor

Seong-Min Kim*, Michael J. McCarthy*, Pictiaw Chen*, Boaz Zion+

*Department of Biological and Agricultural Engineering
University of California at Davis
Davis, CA 95616 USA

+Institute of Agricultural Engineering
Agricultural Research Organization
The Volcani Center
P.O. Box 6
Bet Dagan 50250, Israel

ABSTRACT

A high speed NMR quality evaluation sensor was designed, constructed and tested. The device consists of an NMR spectrometer coupled to a conveyor system. The conveyor was run at speeds ranging from 0 to 250 mm/s. Spectra of avocado fruits and one-dimensional magnetic resonance images of pickled olives were acquired while the samples were moving on a conveyor belt mounted through a 2-Tesla NMR magnet with a 20 mm diameter surface coil and a 150 mm diameter imaging coil respectively.

For a magnetic resonance spectrum analysis, motion through variations in the magnetic field tends to narrow spectral linewidth just like using sample rotation in high resolution NMR to narrow spectral linewidth. Spectrum analysis was used to detect the dry weight of avocado fruits using the ratio of oil and water resonance peaks. Good correlations (maximum r = 0.970 @ 50 mm/s and minimum r = 0.894 @ 250 mm/s) between oil and water resonance peak ratio and dry weight of avocados were observed at speeds ranging from 0 to 250 mm/s.

For the application of magnetic resonance imaging (MRI) method, the projections were used to distinguish between pitted and non-pitted olives. Effect of fruit position in the coil was tested and coil edge effects were noticed when projections were generated under dynamic conditions. Various belt speeds (up to 250 mm/s) were tested and detection results were compared to static measurements. Higher classification errors were occurred at dynamic conditions compared to errors while olives were at rest.

Key Words: Magnetic Resonance, On-line, Fruit, Quality, Sensor, Spectrum, Projection

INTRODUCTION

Nuclear magnetic resonance (NMR) is sensitive to the existence of mobile water. Water is the major component of biological materials. Therefore NMR has a high potential for internal quality evaluation of agricultural products due to its nondestructive nature whenever the component composed of NMR sensitive nuclei is correlated with quality.

The components of fruits change according to their maturation stages. The amount of water, sugar and oil, the most common chemical components of fruits, vary during the ripening process and often relate to the quality factors of the fruit. NMR techniques can detect these chemical components in a non-invasive and non-destructive manner.

For on-line application of NMR techniques, a single pulse spectrum analysis and one-dimensional image analysis are suitable methods for real time sorting. Two-dimensional image acquisition and analysis is possible with proper hardware and software. Using the single pulse spectrum analysis technique Chen *et al.* (1993) determined the oil content of avocados and Zion *et al.*(1995) determined the sugar content of prunes and showed that this method is feasible as an on-line sensor. Zion *et al.* (1994) used a one-dimensional image analysis technique to detect the pits in processed cherries.

Magnetic Resonance Based Sensors

On-line sensors can assist in maintaining product quality and saving processing cost when used for process control. The history of studies concerning on-line magnetic resonance sensors is not long. Few literature studies related to on-line magnetic resonance sensor are available. Most on-line applications studied are related to the determination of the amount of moisture content of the target products. Pearson *et al.* (1987, 1992) developed an in-line magnetic resonance sensor for measuring water and oil contents of wheat and corn. Nicholls and Santos (1991) showed a sampling device for in-line moisture content measurement. Chen *et al.* (1995) demonstrated the feasibility of an on-line NMR fruit quality evaluation sensor.

Magnetic Resonance Spectroscopy (MRS)

When a sample containing nuclear magnetic resonance sensitive nuclei (e.g. ^{1}H or ^{31}P) is exposed to an external magnetic field, the magnetic moments of these nuclei tend to align along the magnetic field direction and precess about their own axes at a specific frequency which is related to the magnitude of applied external magnetic field. The principle of NMR spectroscopy can be expressed as the following equation known as the Larmor relationship:

$$\omega_o = \gamma B_o \ (rad/s) \quad \Rightarrow \quad \nu_o = \frac{\gamma}{2\pi} B_o \ (Hz) \qquad \text{.....(1)}$$

where ω_o is resonance frequency in rad/s, ν_o is resonance frequency in Hz, γ is magnetogyric ratio and B_o is external applied magnetic field strength. From this relationship we can conclude that identical nuclei precess at the same frequency in the same externally applied magnetic field. In a real sample the local magnetic field at each nucleus tends to vary as a result of the local chemical and electronic environment influence on the magnetic field. Therefore, the total effective magnetic field, B_{eff}, caused by these induced currents is expressed

$$B_{eff} = B_o(1-\sigma) \qquad \text{.....(2)}$$

where σ is shielding constant. Combining equation 1 and equation 2 results in a new expression:

$$\nu_o = \frac{\gamma}{2\pi} B_o(1-\sigma). \qquad \text{.....(3)}$$

The magnitude of σ is related to the chemical environment of the nucleus, therefore, proton (^1H) nuclei in oil, sugar, and water generate signals at different frequencies.

Magnetic Resonance Imaging (MRI)

MRI is a collection of experimental techniques which are designed to allow one to measure the NMR properties of a sample as a function of spatial position. The basics of MRI will be explained based on the spin-warp imaging technique. The experiment proceeds by placing the sample in a homogeneous external magnetic field. Pulsed linear magnetic field gradients are used to produce a frequency variations across the sample which can be converted into spatial coordinates. The relationship between frequency and magnetic field is:

$$\omega = \gamma (B + Gx) \quad \text{.....(4)}$$

where ω is the Larmor frequency (rad/sec), G is the linear magnetic field gradient (in Gauss/cm) and x is the spatial distance (cm). For instance, if a linear gradient G is applied in the x direction then the precessional frequency becomes a function of the sum of the homogeneous field and the linear gradient. The frequency spectrum can easily be converted into a position-dependent signal intensity. By the proper application of gradients, one-, two- or three-dimensional mappings of the NMR signal intensity can be recorded (McCarthy, 1994).

The signal, $S(t)$, which is induced in the receiver coil can be expressed in the following equation:

$$S(t) \propto \int_{z=0}^{FOV_z} \int_{y=0}^{FOV_y} \int_{x=0}^{\Delta} \rho(x,y,z) \exp(-i\omega t) dx dy dz \quad \text{.....(5)}$$

where $\omega = \gamma G_z z$, FOV stands for field of view and Δ is slice thickness.

To generate an one-dimensional magnetic resonance image, the time domain data $S(t)$ is arranged as a frequency dependent data set, $S(k)$, in k-space,

$$S(k) \propto \int_{z=0}^{FOV_z} \exp(i2\pi k_z z) \left[\int_{y=0}^{FOV_y} \int_{x=0}^{\Delta} \rho(x,y,z) dx dy \right] dz \quad \text{.....(6)}$$

where $k_z = \gamma G_z t (2\pi)^{-1}$.

The data set $S(k)$ is Fourier transformed to obtain a proton density one-dimensional image (projection),

$$\rho(z) = \int S(k) \exp[-i2\pi(k_z z)] dk_z \,. \quad \text{.....(7)}$$

OBJECTIVES

The objectives of this study were:

- To determine the feasibility of acquiring a single-pulse spectrum and an one-dimensional image from the moving fruit.
- To design and build a conveying system in order to evaluate high-speed NMR techniques for on-line sorting of fruits.

MATERIALS AND METHODS

For MRS sensor application avocados were used due to their high oil content and the availability of results and data related to avocado maturity analysis. Avocado samples (Hass variety) were obtained from a local market in Davis, CA. The correlation of their percentage dry weight to the ratio of oil and water magnetic resonance peaks were studied. For MRI sensor application canned pickled (salted) pitted and non-pitted olives were used as the experimental objects.

Measurement of Percentage Dry Weight

The percentage dry weight (PDW) of an avocado can be used as a maturity index. To determine the PDW of the avocado, a microwave oven (CEM Microwave Drying Moisture/Solids Analyzer, CEM Corporation) was used following the same procedure used by Chen *et al.* (1993).

Spectrum Analysis

NMR spectra of intact avocados were acquired using a 2T NMR spectrometer (General Electric CSI-2) with a 2 cm surface coil operating at a proton resonant frequency of 85.5 MHz. To make the magnetic field homogeneous, first coarse and fine shimming were done with a small water bottle and then again coarse and fine shimming were performed only on the first avocado sample. The resonance spectrum line width of the first sample was 37.4 Hz which is enough to resolve the oil resonance peak. The pulse width was 12 μs, the sweep width was ±1500 Hz, and the complex data size was 2 K (2 K real and 2 K imaginary data was acquired). The free induction decay (FID) signal was obtained from a small region near the surface of the sample by placing the whole sample on the surface coil. The FID signal was Fourier transformed to obtain the FID resonance spectrum, which clearly shows the water and oil resonance peaks.

Projection Analysis

A spin-echo pulse sequence was used to acquire the projections. The slice thickness was 3 mm (in the sagittal plane), the echo delay (TE) was 10 ms, the 180° pulse length was 86 μs, the number of data points in a projection was 128, and the field of view (FOV) in the read-out direction was approximately 147 mm (or 124 mm for three olives), in which case the spatial resolution of the projections was approximately 1.15 mm. The number of acquisitions for signal averaging (NA) was 1. The signal acquired was 'baseline corrected' to reduce the effect of a DC noise component, and multiplied by a trapezoidal window to reduce the effect of high frequency noise components. After performing a 128-point discrete Fourier transform (DFT), the magnitude spectrum was calculated to obtain projections free of phase effects. Olives were placed on the belt on a foam support with their axis perpendicular to the direction of motion. A sagittal imaging plane was chosen with the readout gradient along the direction of motion (the horizontal axis of the magnet) so that projections of olives in the FOV came out side by side. The imaging plane was offset so that it crossed the olives approximately through their center. The magnetic field was shimmed only once, at the beginning of the experiments with a set of five olives in the coil. The projections were analyzed in the same way described by Zion *et al.* (1994).

Instrumentation

The on-line magnetic resonance quality evaluation sensor system consists of two main parts: a conveyor system and a magnet. The conveyor system was designed to convey fruit

samples through the 22 cm diameter bore of the CSI 2T NMR spectrometer. This system, which in shown in Figure 1, is composed of a control unit which contains a programmable controller and motor driver, a stepper motor, and a conveyor.

A BEaR-1FB controller (Blue Earth Research) was used as a controller due to its compactness and practicality. It is a programmable controller which has a ROM containing 8K byte floating point BASIC interpreter and 32K bytes of low power CMOS static RAM usable for program and/or data storage. The BEaR-1FB provides two independent RS-232C compatible communication channels to link with a PC. An IM483 stepper motor driver (Intelligence Motion System, Inc., Taftville, CT) was used to drive a stepper motor at a resolution of 800 steps per revolution. The stepper motor can be controlled to move the conveyor forward or backward at variable speeds and to stop the conveyor at specified locations by the controller. The stepper motor is located at the far end of the conveyor to reduce electrical interference with the magnet. A photo position sensor was used to determine the position of the sample relative to the surface coil. This prototype conveyor was built from nonmagnetic materials. The conveyor was driven by a stepper motor using a rubber driving belt. The conveyor belt was made of nonmagnetic nylon fabric, the rollers were made of Teflon and the conveyor body was made of Plexiglas. Finally, the conveyor system was assembled using Teflon bolts and nuts and supported by wooden frames.

RESULTS AND DISCUSSION

MRS Sensor

Results of experiments conducted with avocado fruits on the moving conveyor show that it is possible to acquire the FID spectrum of a fruit when it is moving on a conveyor belt at speeds ranging from 0 to 250 mm/s. Due to the conveyor belt driving system, the maximum speed was 250 mm/s.

The spectra of each fruit show very little change over this speed range and position variations. The three spectra taken at center position relative to the RF coil at belt speed of 50 mm/s, 150 mm/s, and 250 mm/s are shown in Figure 2. Although peak magnitude and linewidth of each spectrum acquired from a moving fruit were changed slightly we did not observe any significant distortion of the spectrum. Although the linewidth varies with position, it only changes slightly over the entire range of speed for each fruit. The data demonstrate that the linewidth can either increase or decrease with increasing speed. Motion through variations in the magnetic field tends to narrow linewidth just like using rotation of a sample in high resolution NMR to narrow the linewidth.

Linear regression was performed to obtain the correlation between the oil and water resonance peak ratio and the percent dry weight of the fruit for each position and belt speed. The correlation coefficient tends to increase with decreasing belt speed and advance of position. The same trends were observed from the analyses of R_max vs. DW and R_mean vs. DW. Therefore, in R_med and DW analysis the highest correlation coefficient of 0.970 was obtained when the conveyor moved at 50 mm/s and the RF pulse initiated 10 mm before the sample was centered and the lowest correlation coefficient of 0.894 was obtained when the conveyor moved at 250 mm/s and initiated RF pulse 10 mm after the sample center. Figure 3 shows the linear regression fitted lines for the cases of 50 mm/s, 150 mm/s, and 250 mm/s belt speeds. Correlation coefficients were 0.968 (Standard Error of Estimate (SEE) = 1.6625), 0.961 (SEE=1.182), 0.946 (SEE=2.128) for the cases of 50 mm/s, 150 mm/s, and 250 mm/s belt speeds respectively. The sample No. 8 with 43.8% DW was omitted to see the effect of that sample and correlation coefficients were recalculated. The new correlation coefficients were 0.949 (SEE=1.52), 0.948

(SEE=1.530), 0.927 (SEE=1.801) for the cases of 50 mm/s, 150 mm/s, and 250 mm/s belt speeds respectively. With increasing the speeds, however, the correlation coefficients were slightly reduced.

MRI Sensor

The shape of the projection seemed to be slightly different at the five positions because the two side peaks varied in height and the middle peak associated with the pit being hidden or revealed. Those differences may be attributed to noise peaks being added to the olive's projection at random locations, to magnetic field spatial non-homogeneity or to possible misalignment of the conveyor belt with the magnet axis which could offset of the imaging plane with respect to the olive as it changed its position. The projection shape features which were used for quantitative measurement of these changes were the area under the curve (the sum of all the 128 values constructing the projection) and the ratio between the level of the 'valley' or the middle 'peak' and the lower of the two side 'peaks'. The latter (termed "ratio feature") was selected because it was later used for classification of the olives. As expected, the area under the projection curve and the ratio feature were not constant over the five different positions along the coil for the reasons mentioned previously. The standard deviation of the area under the curve ranged from 4.0% to 10.3% of its average over the five positions of each olive. In general, olives at the two positions on the right generated larger projections than when at the two positions on the left. The standard deviation of the ratio feature ranged from 2.7% to 12.2% of its average, however, those variations seemed to be small enough so that the ratio feature of the pitted and non-pitted olives were distinguishable regardless of the position of the olives in the coil while their projections were acquired. Only the lowest ratio feature value of the non-pitted olives (0.737), crossed a possible threshold value of 0.750 below which were the ratios of all pitted olives.

Figure 4 shows projections of a set of three whole (solid line) and pitted (dotted line) olives acquired while traveling through the magnet at three different speeds of 5, 15 and 25 cm/s. The shift to the left in the position of the projection as the speed increased was due to a constant delay between the optical signal that triggers the RF excitation pulses and the beginning of signal acquisition. The shift was in the order of a single pixel (approximately 1 mm) and the speed difference between the projections was 10 cm/s, therefore, the time delay was in the order of 10 ms. This delay was rather long and could be shortened with proper hardware, however, even as it was, the spatial shift could be corrected for (if necessary) by triggering the gating unit earlier so that the projections would be generated in the center of the coil. Another phenomenon observed was a general reduction in signal intensity as a result of increased conveyor speed. The area under the projection curve of the whole set of five olives was used as a measure of the general signal intensity. In all 10 sets there was a decrease in the intensity when the speed was increased from 5 cm/s to 25 cm/s. However, in the first set there was an increase in the intensity and in the second set no change was measured between 5 at 15 cm/s belt speed, while the intensity of the other 8 sets decreased between 6.8% and 20.4%. Similar phenomenon was observed when the area under the projection curves of single olives within the sets were checked. One of the reasons for the decrease in signal intensity generated by moving olives with respect to olives at rest could be the combination of a non-homogeneous magnetic field the motion of spins which together cause dephasing of spins (reduced spins coherence) and increase in signal relaxation rate ($1/T_2^*$). At 25 cm/s, the maximum speed tested, olives moved approximately 1 mm along the coil during signal acquisition duration of 4 ms. Because the imaging coil length was much longer and such a small shift in olives position probably affected very little the projection. The intensity reduction of the first and last olives in each set was larger than that of the three olives in the middle

probably because of coil edge effects since those olives were closer to the edges of the coil than the middle olives. The shape of projections of the first and last olives were distorted by a sharp reduction in the intensity of the side of the projection closer to the edge of the coil. This was more drastic in the projections of the first olives of each set which were traveling towards the edge of the coil while the signal was acquired as opposed to the last olives in the sets which were traveling into the coil. The results of this test indicated that despite the fact that no significant changes in the projection of olives were recorded for various positions along the coil and under static experimental conditions, olives projections were affected significantly under dynamic experimental conditions if their position at the time of signal acquisition was close to one of the two coil edges.

The ability of the algorithm to distinguish between projections of pitted olives and olives with pits which were acquired while they were traveling through the magnet at speeds of 15 cm/s and 25 cm/s was tested with 30 sets of 5 olives, half of which were pitted. The results were compared to those calculated for 10 sets of 5 pitted olives and 11 sets of 5 olives with pits. When the results were analyzed and the projections were plotted, a shift in the position of consecutive sets acquired under static conditions was observed. It was concluded that this undesired shift occurred because the belt slipped when it was driven out of the coil and than back into the coil in order to replace the sets of olives, and therefore, the position of the fifth olive of consecutive sets was gradually shifted out of the field of view. Therefore, the projection of the last olive in all sets acquired under static conditions was disregarded. Considering coil edge effects which were noted in the previous experiment, it was decided to compare the results of the algorithm while disregarding the projections of the first and last olives of all the sets acquired under motion.

There was only a single pitted olive whose two-peak projection ratio feature (the ratio between the valley and the lower peak) was high so that it overlapped ratio feature values of olives with pits. Had a threshold value of 0.720 was chosen for the two-peak projections to distinguish between olives with pits and pitted olives, only one misclassification would occur. The ratio feature of the single pitted olive which generated a three-peak projection was much lower than those of the olives with pits and therefore easily distinguishable. In addition, one of the pitted olives generated a single-peak projection and therefore misclassified as a non-pitted olive. Altogether, only two out of 84 olives were misclassified under static conditions. At 15 cm/s, two pitted olives and two non-pitted olives which generated two-peak projections were misclassified (with respect to a threshold value of 0.720), as well as two pitted olives which generated three-peak projections (with respect to a threshold value of 0.750). Altogether 6 out of 45 olives were misclassified at 15 cm/s belt speed. At 25 cm/s belt speed, the ratio features of pitted and non-pitted olives which generated two-peak projections were completely separable by a threshold value of 0.748, and two pitted olives which generated three-peak projections were misclassified by a threshold value of 0.750. Altogether 2 out of 45 olives were misclassified at 25 cm/s belt speed.

The results achieved under static conditions were slightly better (2.4% classification errors) than those reported by Zion *et al.* (1995) for processed cherries (3.3% classification errors). Under dynamic conditions, detection errors increased to 13.3% and 4.4% at 15 and 25 cm/s belt speeds, respectively. It is not clear at this point whether the errors were due to motion effects or due to experimental errors and the experiments are planned to be repeated and with a larger sample of olives.

The time taken to generate a projection of a set of olives (including excitation and signal acquisition) was less than 5 ms and therefore, data processing and analysis become the limiting time factors for a high detection rate operation. At 25 cm/s belt speed a throughput of approximately 10 olives per second may be feasible (assuming an olive occupies 2.5 cm on the

belt including a necessary gap between neighboring olives). Testing the method at higher belt speeds is planned.

CONCLUSIONS

From the results of MRS sensor study the following conclusions can be drawn:

1. Motion of avocados over the surface coil, at speeds up to 250 mm/s, does not change the acquired FID.
2. There is small variation in correlation coefficient with position differences within ±4 mm of the coil center.
3. Good correlations (max. r = 0.970 @ 50 mm/s and min. r = 0.894 @ 250 mm/s) between oil and water resonance peak ratio and dry weight of avocados are observed.
4. The results of this research demonstrates the feasibility of an on-line NMR based sensor for detecting internal quality of avocados.

From the results of MRI sensor study the following conclusions can be drawn:

1. Motion of olives inside the birdcage coil, at speeds up to 250 mm/s, does not change the acquired projection.
2. As the speed of the olives traveling through the magnet increased, the signal they generated becomes weaker.
3. It is found that the ratio feature (the ratio of the valley or middle peak to the lower of the two side peaks of two-peak and three-peak projections, respectively) varied little enough to enable differentiation between pitted and non-pitted olives regardless of their position.
4. Even though the number of classification errors increases under dynamic conditions the performance of this method can be considered good.

The results of this research demonstrated the feasibility of an on-line NMR based sensor for detecting internal quality of fruits. For an on-line NMR based sensor, more studies are needed on the conveyor design and control, and sorting algorithms. NMR based sensors coupled with external quality evaluation sensors should be studied for the future development of a complete sorting and grading machine that can evaluate internal and external qualities simultaneously.

SIGNIFICANCE OF FINDINGS

In this study we have shown for the first time that it is possible to acquire an NMR signal from moving fruits. Moreover, we discovered that when the RF pulsing is made at the right moment, the NMR signal acquired from fruits moving at speeds up to 250 mm/s is essentially identical to that obtained from the fruits while they are stationary. This accomplishment is an important step toward the development of on-line sorting of fruits and vegetables.

ACKNOWLEDGMENT

This research was supported by Grant No. US-2312-93RC from BARD (The United States-Israel Binational Agricultural Research and Development Fund).

REFERENCES

1. Chen, P., M.J. McCarthy, and R. Kauten. 1989. NMR for internal quality evaluation of fruits and vegetables. Transactions of the ASAE 32(5):1747-1753.
2. Chen, P., M.J. McCarthy, R. Kauten, Y. Sarig, and S. Han. 1993. Maturity Evaluation of Avocados by NMR Methods. J. Agric. Engr. Res. 55:177-183.
3. Chen, P., M.J. McCarthy, S.M. Kim and B. Zion. 1995. Development of a High-Speed NMR Technique for Sensing Fruit Quality. ASAE paper No. 95-3613.
4. Heil, J.R., K.L. McCarthy, J.B. German, and M.J. McCarthy. 1991. Use of magnetic resonance imaging for evaluation of beer foam characteristics. The American Society of Brewing Chemistry, 48(4):119-122.
5. McCarthy, MJ. 1994. Magnetic Resonance Imaging in Foods. Chapman & Hall, New York, NY.
6. Nicholls, C., and A. De Los Santos. 1991. Hydrogen Transient Nuclear Magnetic Resonance for Industrial Moisture Sensing. Drying Technology. 9:849-873.
7. Pearson, R., L. Ream, C. Job, and J. Adams. 1987. The Use of Small Magnetic Resonance Spectrometers for On-line Process Control. Cereal Foods World. 32:822-826.
8. Pearson, R., and C. Job. 1992. Process Control by Nuclear Magnetic Resonance. Food Processing Automation II. ASAE. 40-47.
9. Tellier, C., and F. Mariette. 1995. On-line Applications in Food Science. Annual Reports on NMR Spectroscopy. Vol. 31:105-122.
10. Zion, B., M.J. McCarthy, and P. Chen. 1994. Real-time detection of pits in processed cherries by magnetic resonance projections. Lebensmittel-Wissenschaft und-Technologie (Food Science and Technology) 27(5):457-462.
11. Zion, B., P. Chen, and M.J. McCarthy. 1995. Non-destructive quality evaluation of fresh prunes by NMR spectroscopy. Journal of the Science of Food and Agriculture 67:423-429.

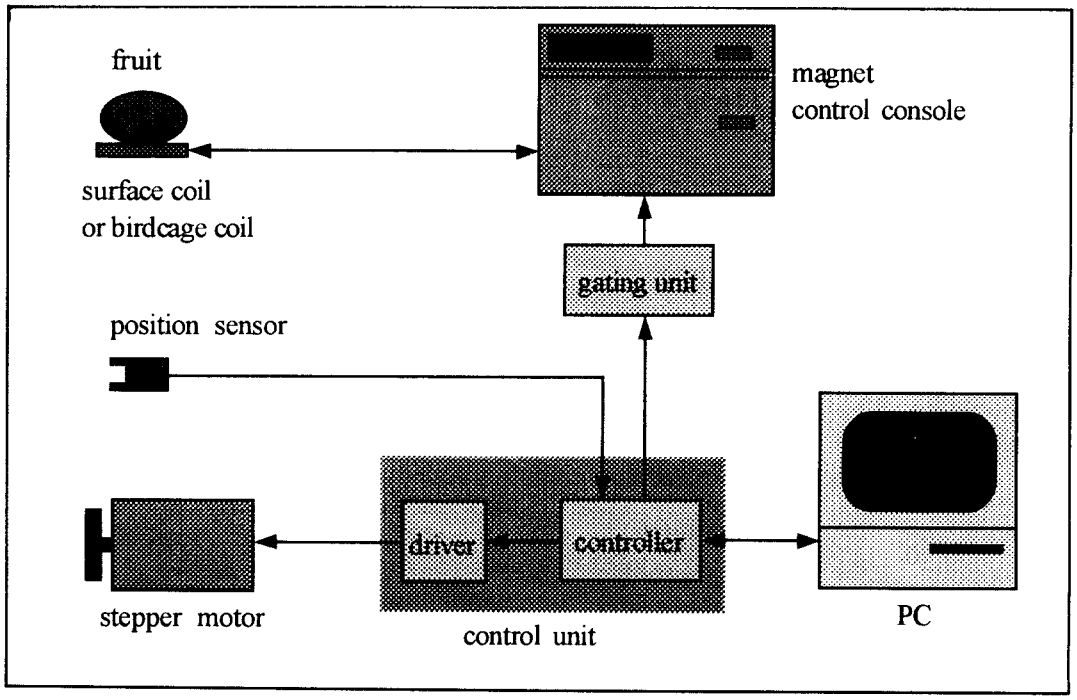

Figure 1. Schematic diagram of on-line MR sensor.

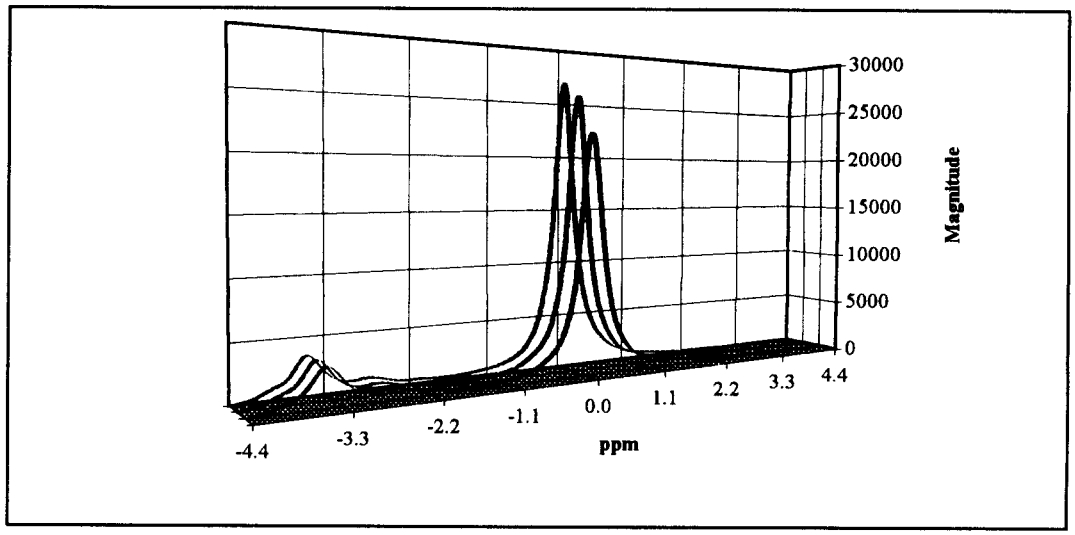

Figure 2. Spectra of an avocado acquiring as it moves on a conveyor at three speeds, 50 mm/s, 150 mm/s, and 250 mm/s from back to front, respectively.

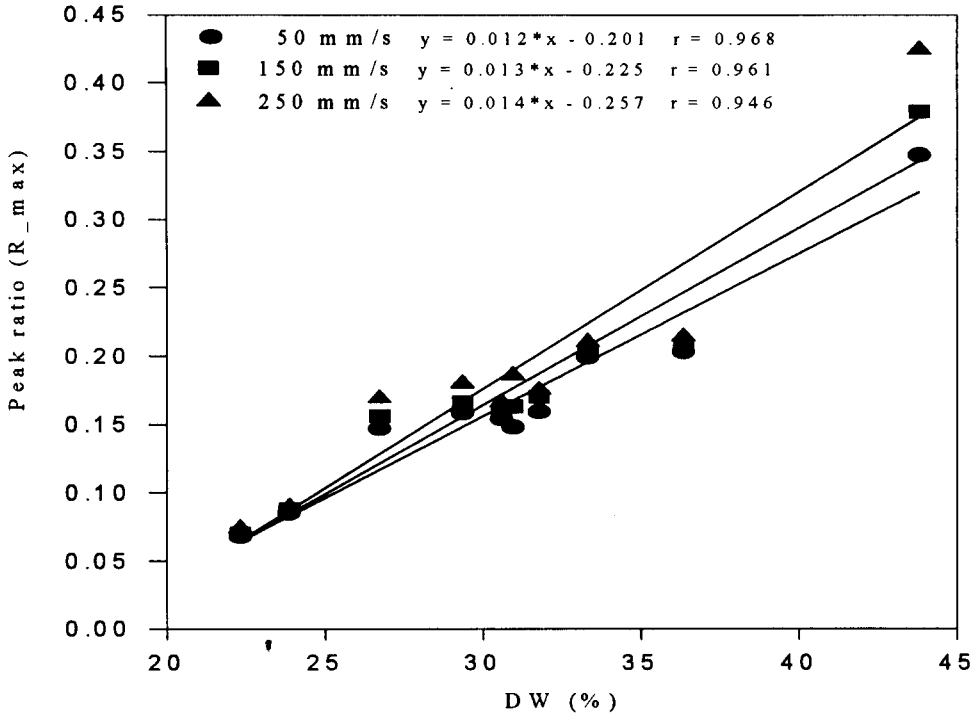

Figure 3. Linear regression plot between oil and water resonance peak ratio (R_max) and fruit dry weight (%) showing small differences with different belt speeds ranging from 50 mm/s to 250 mm/s.

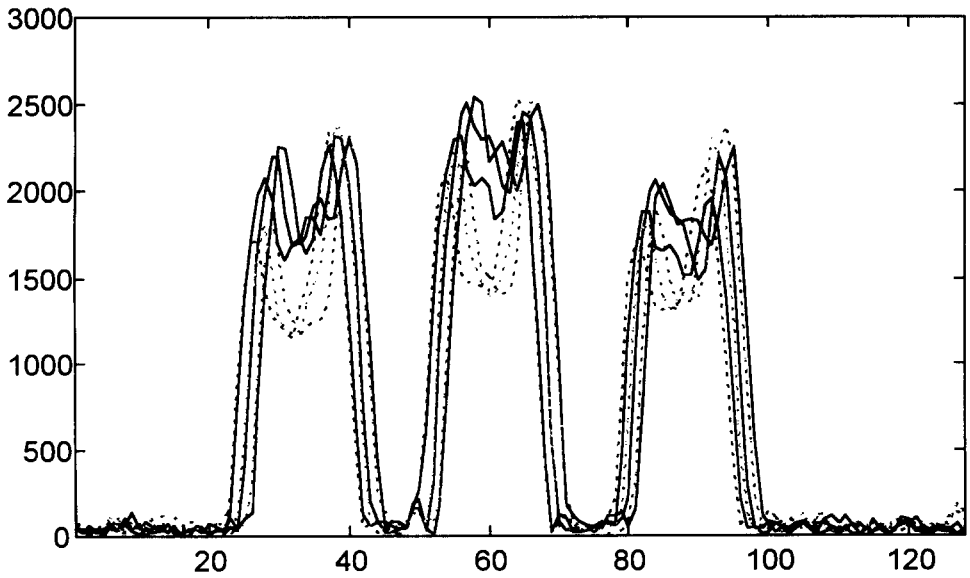

Figure 4. Projections of a set of three whole (solid line) and pitted (dotted line) olives acquired while moving through the magnet at three different speeds of 5, 15 and 25 cm/s.